Journal of Computational Physics **161,** 21–34 (2000)
doi:10.1006/jcph.2000.6442, available online at http://www.idealibrary.com on IDEAL®

MINI REVIEW

Computer Modeling in Cardiac Electrophysiology

Niels F. Otani

Department of Biomedical Engineering, Case Western Reserve University, Cleveland, Ohio 44106

Received June 15, 1998; revised December 27, 1999

The skills of a computational physicist are shown to be useful in the seemingly distant field of cardiac electrophysiology. The propagation of cardiac action potentials and their ability to form spiral waves are easily understood at a basic level when standard concepts from the theory of partial differential equations are applied. The design of computer simulations of action potential propagation is facilitated by adapting numerical concepts routinely applied by computational physicists. These concepts must be modified and combined with computer structures standard in computer science to handle the timescale and spatial scale problems unique to the action potential propagation problem. The resulting simulation shows how details of ion channel dynamics determine properties of the spiral wave, including its propagation speed, its period, its stability, and the size of the spiral core.

1. INTRODUCTICON

The ideas and concepts commonly employed by computational physicists in the design of numerical models and in the analysis of the simulation results find application well beyond the areas traditionally assigned to physics and applied physics. In this paper, I describe my experiences as a newly transplanted (pun is intentional) computational physicist into the world of cardiac bioelectrical modeling, one such peripheral field. This article is thus *not* a review, but instead a personal perspective. A surprisingly broad range of skills commonly held by the computational physicist turn out to be applicable here, with many concepts from numerical analysis, physics, and computer science not only being useful, but also providing an unusual and insightful perspective on many topics within the field. Of course, this is not to minimize the importance of the immense body of knowledge underlying the two other fields, physiology and cardiology, which are absolutely essential in this type of research. In the following, I will concentrate on one particular active research area in

0021-9991/00 $35.00

cardiac bioelectricity, that which seeks to understand how cardiac action potentials, waves of electrical activity on the heart, propagate. The study of the properties of action potentials is important, because disruption in their normal behavior is one of the principal killers in the United States, causing between 200,000 and 400,000 deaths a year, both in association with, and independently of, heart attack and related cardiac diseases.

2. WHAT MAKES AN ACTION POTENTIAL PROPAGATE?

The general theory of action potential propagation is well known. The basic principles appear in any good physiology textbook, for example, [11]. Additional technical detail may be found, for example, in [32]. Briefly, heart muscle is composed of many long relatively thin cells ($\approx$100 by 20 μm) which are oriented roughly parallel to one another. A thin membrane encapsulates each of these cells. This membrane is, for the most part, an insulator, and thus is capable of supporting a potential drop between the inside and the outside of the cell. This voltage is called the membrane potential V, as depicted schematically in Fig. 1. The membrane also separates various types of ions, including sodium, potassium, and calcium ions, which typically have different concentrations inside and outside the cells. Embedded in the membrane are *ion channels*, which, when open, selectively allow passage of one or more ion species (Fig. 1). Through numerous experiments, researchers have found that, for most ion channels, a subset of the membrane voltage, the ion concentrations, the pH, and/or other quantities determines the rates at which channels open and close. In turn, the fraction of the various types of channels which are open at any given time determines the instantaneous current passing through the membrane. These currents, along with the currents which flow internally along the length of the cell and currents which flow outside the cell, determine the membrane potential and the internal and external concentrations at every point along the cell.

Clearly, then, if quantities such as the pH and the external concentrations are so slowly varying that we can assume them to be constant, then we have a self-consistent system, with the ion currents determining the internal ion concentrations and membrane voltage, and the concentrations and voltages determining the currents through control of the ion channels. For many of the tissues in the heart, the nature of this regulation is so as to make the cells *excitable*—that is, if the membrane voltage is raised above a certain critical value, then many of the channels in the cell, most notably the sodium channels, open, creating a large inward

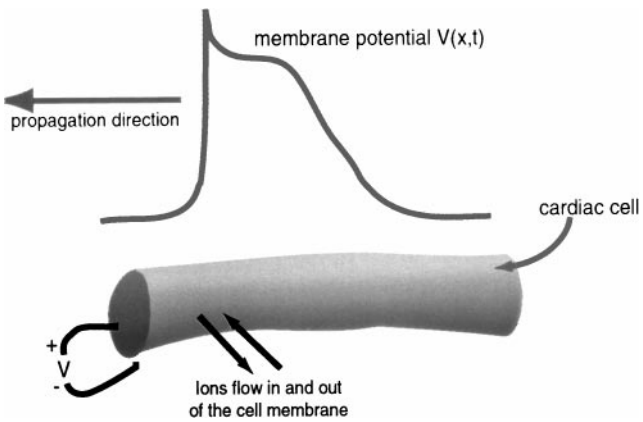

FIG. 1. Propagation of an action potential along a cardiac cell.

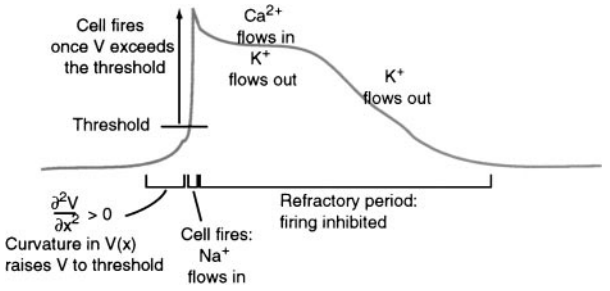

FIG. 2. Dynamics of the formation of an action potential.

current, forcing the membrane voltage very rapidly upward (Fig. 2). Following the firing phase, more commonly called the *upstroke* or *depolarization* of the cell, the sodium channels close, while potassium and calcium channels slowly open. Since potassium concentrations are typically higher inside, while the reverse is true of calcium, the current associated with these two ion species roughly cancel, which maintains the membrane potential at a near-constant value. This phase is called the plateau phase, illustrated in Fig. 2. Soon thereafter, the calcium channels close while potassium channels remain open. The membrane current is now dominated by outward flowing potassium ions, which repolarizes the cell back to its rest potential. The depolarization and subsequent repolarization of a cell in response to a positive shift in the membrane voltage is referred to as an *action potential*. Action potentials initiate, through a series of events internal to the cell, a mechanical contraction of the cell principally along its length. It is this ability of the cells to contract in concert with other cells that is responsible for the ability of the heart to pump blood.

Once the sodium channels close following their part in initiating the upstroke, they are inhibited from opening again for a period which is typically comparable to, or slightly longer than, the duration of the action potential. When a cell's sodium channels are inhibited from opening, the cell is said to be in a *refractory* state. The inability of a cell to fire immediately after it has just fired is an important property, as we shall see later.

This description of the generation of an action potential neglects currents which flow entirely outside the cell, or entirely inside the cell, along its length. The description is therefore a local one, focusing essentially on one cell or a small group of cells. While, in many cases, we can consider the region outside the cell to be effectively a constant potential region, essentially a system ground, the voltage drops associated with the current flows inside the cells and between cells are typically important. For our purposes, the cardiac cell interiors may be thought of collectively as a uniformly resistive medium. The intracellular current is thus proportional to the gradient in membrane potential, $\partial V/\partial x$, where x is a spatial coordinate along the length of the cell. Charging of the membrane at a particular point x along the cell can therefore occur when current is flowing into the point x, say, from the right, but not from the left. It is therefore the change in $\partial V/\partial x$ with x, that is, $\partial^2 V/\partial x^2$, which contributes to charge buildup and therefore membrane potential buildup $c\partial V/\partial t$, at a particular point x, where c is a constant proportional to the membrane capacitance. Current flowing through the membrane at the point x also contributes to the change in membrane potential, as we have seen above, so the equation governing the membrane voltage at point x along the length of a cell is

$$\frac{\partial V}{\partial t} = \frac{\partial^2 V}{\partial x^2} - I_{\text{ion}}, \tag{1}$$

where all the constants have been suppressed. I_{ion} includes all the local channel currents discussed earlier. In two or three spatial dimensions, $\partial^2 V/\partial x^2$ is replaced by $\nabla \cdot (\sigma \cdot \nabla V)$, where σ is an electrical conductivity tensor representing the intracellular medium.

Consider now what happens if, as shown in Fig. 2, an action potential upstroke has just occurred just to the right of a point x, but cells are at rest at x and leftward of x. The $\partial^2 V/\partial x^2$ term is then positive at x, causing the voltage V to rise in Eq. (1). Once this voltage reaches the threshold, the corresponding cell fires, as represented by a large negative sodium current appearing in I_{ion}, and the action potential has effectively been propagated one step to the left. A point just to the left of x now is in a similar predicament as the point x was in a moment ago and will be the next to fire.

This is the mechanism by which action potentials, and therefore waves of mechanical contraction, propagate in the heart. The governing equations are Eq. (1) together with the equations which determine I_{ion}. When the $\partial^2 V/\partial x^2$ term is ignored, the equations are essentially those of a dynamical system describing the local behavior of the cell. The tools of nonlinear dynamics are therefore relevant, and have already contributed substantially to our understanding of excitable tissue behavior when applied to local models of cardiac cells and ion channels. When the second derivative is reinstated, the equations are essentially of the reaction–diffusion type, which, interestingly, allow unattenuated wave propagation, even though the equations are essentially parabolic and therefore diffusive in nature. These waves are distinctly different from those typically appearing in hyperbolic systems. When two action potentials waves meet head-on, they annihilate, rather than pass through, each other. Also, when an action potential encounters the edge of a system (which, in the heart, would represent some anatomical object, such as a large blood vessel) it is annihilated instead of reflected.

3. SPIRAL AND SCROLL WAVES

Perhaps the most interesting wave patterns supported by these equations are the so-called *spiral* and *scroll waves*, in two and three dimensions, respectively ([3, 13, 30]; see the reference list in [29] and [4]). Although these waveforms are still a topic of controversy, many researchers believe that they are responsible for a number of different cardiac arrhythmias, including some which are often fatal.

Figure 3 shows one method by which these waves might be formed. Suppose, as shown in the upper panel, a plane action potential wave is propagating upward. Next, suppose that, just behind this wave, a group of cells fires abnormally, as is known to happen in some situations in the heart. Cells above this abnormal firing region are still in the refractory state, due to the recent passage of the original action potential plane wave. The abnormal cell group therefore excites a wave which can only propagate downward and sideward, as shown. Soon, however, the rightward propagating portion of this second wave finds that the cells above it are no longer refractory and thus have recovered their ability to fire. This portion of the wave can now enter this region propagating upward, and soon leftward, as shown in the middle panel of Fig. 3. Meanwhile the downward portion of the wave has now generated its own region of refractory cells, which follows the wavefront. As these cells recover, the upward and leftward propagating portion of the wave soon finds that it can now follow this formerly refractory region downward and then rightward. Clearly, this process can continue, forming the spiral wave pattern shown in the lower panel.

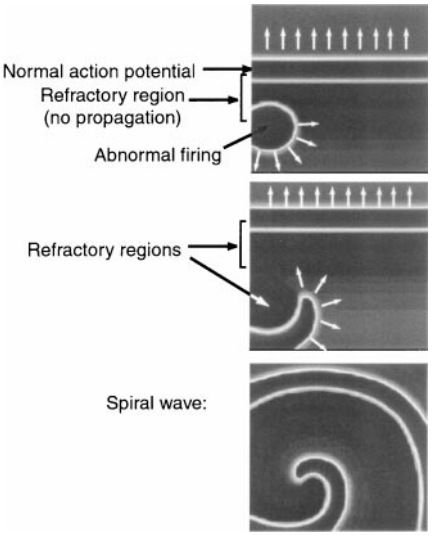

FIG. 3. One means by which a spiral wave may be produced. Results are taken from a simulation based on a standard simplified model for excitable dynamics due to [9, 18].

Assuming that such patterns actually form in the heart, they would likely pump much less efficiently than the normal wave pattern, which would lead quickly to oxygen deprivation in all parts of the body, including the heart itself. The lack of oxygen changes the electrical properties of the cardiac cells, which could lead to further anomalies and more complicated, and therefore more serious and possibly lethal, action potential wave patterns.

It is still not clear whether spiral waves are the principal cause of so-called "functionally reentrant" arrhythmias. Other patterns of circulating action potentials, possessing different dynamic properties, are also possible, including those caused by leading-circle reentry [1], figure-of-eight reentry [7], and anisotropic reentry [5].

Simulations of various types have been designed to study these various propagation patterns. Bidomain models (e.g., [24, 26]) take into account the regions both inside and outside the cardiac cells. The conductivity of the extracellular space is regarded as finite in bidomain models, not infinite, as is typically assumed by other types of models, often an important effect. Other types of models use finite element [23] or finite volume [12] methods to allow flexibility in specifying the spatial structure of the tissue. Still others explicitly take into account the anatomical structure of cardiac muscle as bundles of fibers [15, 28] or model explicity the fundamentally three-dimensional nature of ventricular myocardium. Spiral waves in particular also exist in three dimensions, as shown in Fig. 4, where they are generally referred to as scroll waves [8, 14].

4. NUMERICAL ISSUES IN DETAILED MODELS

Another area of current interest has to do with which aspects of ion channel dynamics are operative in spiral waves and other reentrant patterns when all the details of realistic ventricular muscle are included. Are spiral waves still possible? What kind of dynamics will exist at the center of the spiral pattern? Will these dynamics, as well as the dynamics

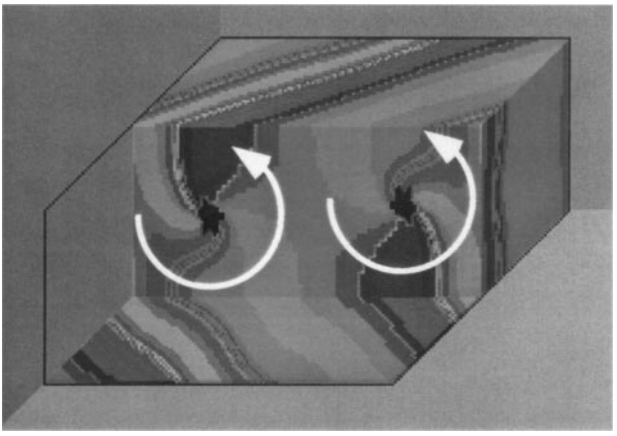

FIG. 4. Example of two scroll waves in three dimensions. Reprinted from [19] with permission from Elsevier Science.

of the pattern as a whole, be stable? This topic is, in particular, important in the formulation of drug therapies, since drugs directly target the dynamics of ion channels. To answer these questions, we need a detailed comprehensive model of the local dynamics. Fortunately, one exists: the Luo–Rudy dynamic (LRd) model [16, 17, 31] which contains over 60 nonlinear equations describing the flow of ions through specialized channels in the cell membrane, as well as dynamics of the intracellular ion concentrations.

Incorporating this type of model into a two- or three-dimensional spatial model presents a couple of numerical challenges. One numerical complication simply concerns the time required to evaluate over 60 equations each timestep at each computational node. The other complication has to do with the existence of disparate timescales. The rapid upstroke of the action potential requires a timestep on the order of microseconds, while the remainder of the action potential develops on a relatively slow timescale (2 ms to 1000 ms and slower). The timescale separation problem in action potential modeling differs from the one found in many hyperbolic equation models such as those found in plasma physics, fluid dynamics, and electrodynamics. In the latter, many types of waves are present simultaneously, with widely differing characteristic temporal and spatial scales. In contrast, in the cardiac electrophysiology, action potential waves are typically the only waves present, and their fast timescales appear only very briefly, during the action potential upstroke. Elsewhere, the dynamical variables evolve on a much slower timescale, although the underlying equations still contain fast, albeit unexpressed, timescales.

We can deal with a portion of this problem by using what is called the hybrid method in this field. (This method is unrelated to the hybrid method as defined in plasma physics.) The fast timescales in our system come from the dynamics of the so-called gating variables, quantities which are associated with the opening and closing of the ion channels. The equations governing these variables are of the form

$$\frac{dy}{dt} = -\frac{y - y_\infty(V)}{\tau_y(V)}, \tag{2}$$

where y is any of several gating variables, and both the equilibrium value y_∞ of y and the characteristic timescale τ_y depend on the membrane potential V. In the hybrid model, this

equation is advanced from timestep n to timestep $n+1$ using the formula

$$y_{n+1} = y_\infty(V_n) + \Delta t(y_n - y_\infty(V_n))e^{-\Delta t/\tau_y(V_n)}. \tag{3}$$

This formula would, of course, be exact for any value Δt if V were constant. This property of Eq. (3) not only limits the computational errors to those coming from the time dependence on V, but also eliminates any numerical instability associated with the advance of the gating variables, as would be the case, for example, if the forward Euler method were used. Use of this method, however, does not rule out the possibility of numerical instabilities arising from the interaction of these gating equations with other equations. In our code, we use the hybrid model for the gating equations and the forward Euler method for the remainder of equations involving time derivatives.

The remaining timescale disparity problems can be handled by implementing a variable timestep method. Since, at different times, the upstroke of the propagating action potential is present at different places in the simulation system, we in general must require that each node in the simulation grid have its own timestep and have the ability to modify this timestep as the simulation runs. In single cell simulations, Rush and Larsen [25] adjusted the timestep in proportion to $(dV/dt)^{-1}$ within some large range (e.g., between 10 μs and 1 ms). This condition derives from the fact that dV/dt is typically largest in the action potential upstroke, during which, coincidentally, the use of a small timestep is most important. Another common method chooses the timestep from two or three values [27, 28]. The eligible values are often chosen to be integer multiples of each other, to simplify the bookkeeping. Another method divides the simulation region into several subdomains, and then chooses a single, variable timestep for each of these regions [22]. The timestep for each region is chosen based on conditions which are associated with the proximity of the region to the action potential upstroke, either temporally or spatially.

In our simulations, we tried applying the idea of a continuously varying timestep to each cell in our two-dimensional simulation. Each timestep was determined according to a prescription suggested by Gear [10], using the variables we know are associated with the fastest timescale: the membrane potential V and the fastest gating quantity in the problem, the sodium activation gate, m. Since our overall method is first-order in time, the error and therefore the timestep are defined in terms of the second time derivatives:

$$\Delta t = [\min\{\epsilon_V/|\partial^2 V/\partial t^2|, \epsilon_m/|\partial^2 m/\partial t^2|\}]^{1/2}. \tag{4}$$

Here ϵ_V and ϵ_m are the error tolerances we set for V and m, respectively. Since the second derivative is itself approximated by finite differencing with a timestep Δt, the timestep must occasionally be adjusted more than once for a given time advance to obtain consistency between the value Δt obtained from the left-hand side of Eq. (4) and the one used in calculating the time derivatives.

A drawback to this individually variable timestep method is that it is difficult to implement implicitly. Use of an implicit method is sometimes important when spatial resolution issues require that a small cell size be used. The diffusion term in Eq. (1) in particular can impose a severe constraint on the timestep in these circumstances if explicit methods such as the forward Euler method are used. The problem is that implicit methods such as the Crank–Nicolson and backward Euler methods generally operate on all the cells at once and return values defined everywhere at the same time. Simulations by Pollard *et al.* [20],

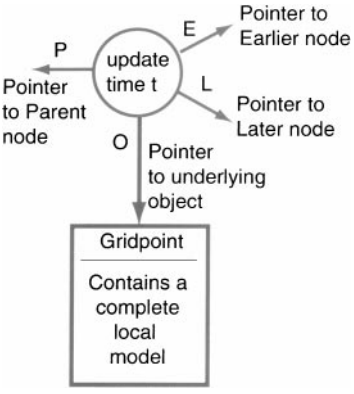

FIG. 5. Structure of a node used in the binary tree updating scheme.

Shaw and Rudy [27], and Quan *et al.* [22], which used implicit methods, were therefore required to use a single timestep across the entire system for those portions of their algorithms which treated the diffusion term implicitly. This timestep was constrained to be the smallest timestep needed for whatever reason by any cell in the simulation at the current time.

When this variable timestepping method is applied to a system of coupled nodes, two new problems arise: how to schedule timestep advances among the various nodes, and how to calculate the second spatial derivatives (such as the one appearing in Eq. (1)) which couple adjacent nodes in the simulation grid.

Since, at any particular point in the simulation, different nodes will have been advanced to different times, it becomes a bit of a problem to decide which node to update next. The next node to update is always the one furthest behind in time. To keep track of which node this is, we use a scheduling algorithm based on a binary tree, a standard technique in the field of computer science. Each node of the binary tree (to be distinguished from the nodes of the simulation grid) contains the current time t of the node, and a maximum of four pointers: a parent node pointer (P), two child node pointers, one called "earlier" (E) and one called "later" (L), and a pointer to the simulation node (O), as shown in Fig. 5. Not every pointer is defined for every binary tree node.

Once the binary tree nodes are created, their pointers are defined to form the tree structure shown in Fig. 6. The time t associated with the nodes whose O-pointers are pointing at simulation nodes (the rightmost nodes in Fig. 6) is defined to equal the current time of the

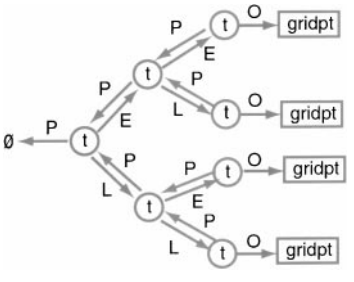

FIG. 6. Structure of nodes in the binary scheduling tree.

simulation node its O-pointer points at. The E-pointer of the other tree nodes points at the earlier of the two nodes pointed at by the E- and L-pointers, defined as the node having the earlier time t, while the L-pointer points at the later of these two nodes. The time t associated with these nodes is defined to be equal to the time t associated with the node pointed to by the E-pointer.

After the tree is defined in this way, one need only follow the E-pointers starting at the trunk node (the leftmost node in Fig. 6) to find the next simulation node to update.

Once a simulation node is updated, the tree must be modified to reflect this node's new current time. This is accomplished by (1) updating the tree node's value of t for the simulation node just advanced, (2) following that node's P-pointer back to the parent node, (3) updating this parent's node's value of t with the earlier of the times E and L point at, (4) switching E and L if necessary, and (5) repeating (2), (3), and (4) until the trunk of the tree is reached.

C++ is a particularly convenient language for implementing this scheduling tree, both for defining these nodes and the node tree, and for defining the functions which make the tree useful. This scheduling algorithm scales like $\log_2 N$ per update, N being the number of simulation nodes.

The other problem created by multiple, variable timestepping has to do with evaluating $\nabla \cdot (\sigma \cdot \nabla V)$, the term associated with intracellular or intercellular (gap-junction) resistive coupling. Suppose that our simulation grid is two-dimensional and rectangular in space, and that the next simulation node to update is the one located at gridpoint (i, j). Our update algorithm, as just described, requires that the current time t of this gridpoint must be simultaneous with or earlier than all other gridpoints in the simulation, including in particular the adjacent gridpoints. This situation is depicted in Fig. 7, with the current time of the (i, j)th gridpoint and adjacent gridpoints denoted by filled circles. Also, it should be clear that, with this "earliest-node" scheduling algorithm, all previous times of all the nodes in the simulation must be earlier than the current time of node (i, j). This applies in particular to nodes adjacent to node (i, j) evaluated at times t one timestep prior to their current times, as denoted by the open circles in Fig. 7. Linear interpolation (as opposed to extrapolation) to evaluate the membrane voltages V at the current time of node (i, j) is therefore possible, as denoted by the diamonds in Fig. 7. Calculation of $\nabla^2 V$ at the current time t at node (i, j) can then proceed in the standard way using these interpolated adjacent

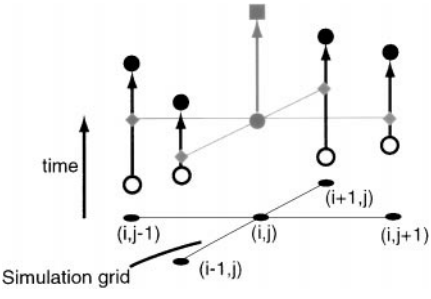

FIG. 7. Interpolation scheme used to calculate the $\nabla^2 V$ term when individual cells are advanced using a variable timestep method. The vertical direction represents increasing time t, while the horizontal directions represent the two spatial dimensions of the simulation. The simulation grid is shown beneath the interpolation scheme, for reference.

node voltages

$$\nabla \cdot (\sigma \cdot \nabla V) \approx \sigma_{ii} \frac{V^{\text{interp}}_{i+1,j}(t) - 2V_{i,j}(t) + V^{\text{interp}}_{i-1,j}(t)}{\Delta x^2} + \sigma_{jj} \frac{V^{\text{interp}}_{i,j+1}(t) - 2V_{i,j}(t) + V^{\text{interp}}_{i,j-1}(t)}{\Delta y^2}, \quad (5)$$

where σ_{ii} and σ_{jj} are the conductivities, and Δx and Δy are the simulation grid spacings, in the i and j directions, respectively. These directions are assumed to lie along the principal axes of the conductivity tensor σ.

5. SOME RESULTS

Preliminary simulations have been conducted employing these numerical techniques. We used a rectangular grid, 256 by 256 cells, with equal spacing and equal resistances coupling adjacent cells each direction. Cells were chosen to be 293 μm square. The simulation cells were thus larger than actual cells. This is computationally and physiologically acceptable, since the dimensions of both our simulation cells and actual cells are much smaller than the characteristic length scale in this problem (about 1 mm). Other parameters were chosen to represent normal cardiac tissue. The accuracy of the model was tested by measuring the propagation speed of a plane wave action potential traveling into a region of cells sitting at the rest potential. We find that the propagation speed varies less than 2% when either the grid spacing or the timestep error parameters ϵ_V and ϵ_m are decreased by a factor of two. The propagation speed obtained, 49 cm/s, is comparable to that obtained in normal ventricular tissue.

We next created a spiral wave by first initiating a propagating action potential from the bottom of the system and then starting a second potential from the left side of the system, after a delay of 220 ms. The results are summarized in Fig. 8.

When viewed in terms of the intracellular calcium concentration (Fig. 8a), the spiral wave has a substantial central "core" region, a relatively quiescent region surrounding the center of rotation, an eye for the spiral wave hurricane, around which the wave rotates. In contrast, when viewed in terms of the membrane potential (Fig. 8b), no such core region exists—the action potential extends right up to the center of rotation. As we have come to expect of computational methods, one of the major benefits of simulation is that we have access to all the variables everywhere in space and time, and thus have all the tools necessary to construct a complete picture of the underlying process. In this case, the "calcium core" may be explained by a short sequence of events, which, despite its simplicity, illustrates the detailed and comprehensive nature of the LRd model and the interdependence of its many parts.

We start by examining the time history of the membrane at several locations close to the center of rotation (Fig. 8c). The trace taken closest to the center shows near-sinusoidal behavior with a minimum (-58 mV) well above the resting potential of the cell (-86 mV). This time-averaged elevation of the membrane potential comes about through the "electronic effect," that is, the action of the diffusion term appearing in Eq. (1) spreading the higher membrane potential associated with the nearby rotating action potential into the core region. It is well known that elevated membrane potentials like this inactivate, that is, turn off, the sodium channels, the key players in producing the action potential upstroke, as we have already discussed. It is still possible for the cell to generate something resembling

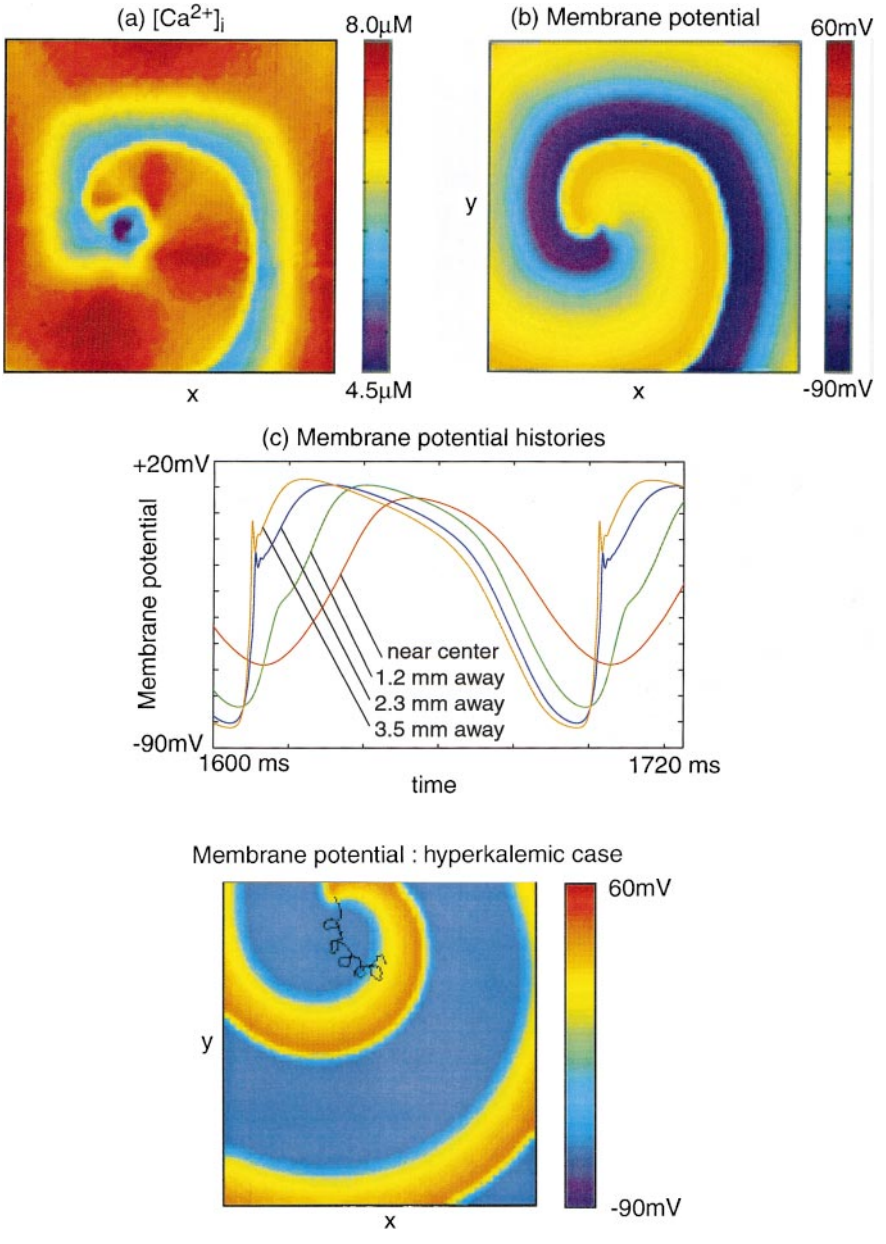

FIG. 8. Simultaneous snapshots of (a) the intracellular calcium concentration and (b) the membrane potential from a 2-d LRd simulation of normal ventricular myocardium. (c) Plots of the membrane potential vs time at different distances from the center of rotation of the spiral wave from the same simulation.

FIG. 9. Snapshot of the membrane potential from a two-dimensional LRd simulation of hyperkalemic tissue ($[Ca^{2+}]_i$). The curly black line represents the trajectory of the spiral tip.

an action potential using its L-type calcium channels in place of sodium channels, as is probably occurring in the action potential trace 1.2 mm from the core center in Fig. 8c. This action potential, however, possesses a much slower upstroke than one produced by sodium. For example, compare this upstroke to one driven by substantial sodium influx 3.5 mm from the core in Fig. 8c. In a normal upstroke, the rapid change in membrane potential induces a substantial release of calcium into the main intracellular compartment from the sarcoplasmic reticulum, a structure internal to the cell. The lack of sodium current near the center of rotation removes this mechanism from the core region. The intracellular calcium concentration thus remains low at and near the center of rotation compared to the surrounding area, forming the calcium core region seen in Fig. 8a.

We also conducted other simulations to get a feeling for the scope of possibilities. When the extracellular potassium concentration is raised to 14 mM (hyperkalemia) from a normal value of 5.4 mM, for example, the result is a spiral wave with a strikingly different appearance (see Fig. 9). Rather than rotating around a single fixed location, the tip of the spiral wave traces out a flower-shaped pattern. This behavior, called meandering, has also been observed in other spiral wave models [2, 6]. Other features of note are a slower propagation speed (11 cm/s vs 37 cm/s), slower rotation speed (a period of 300 ms vs 90 ms), and a much longer period between action potentials (180 ms vs 15 ms). This last distinction also turns out to be important—if the interval between action potentials is short, the interaction between the head and tail of the action potential is strong, which can lead to instability and possible termination of sections of the wavefront. The surviving wavefront segments often form more spiral waves centered around their newly created endpoints. The repetitive occurrence of this sequence of events is called spiral wave breakup [21] and generally leads to a very complicated propagation pattern many believe is associated with ventricular fibrillation, among the deadliest of cardiac arrhythmias.

We also tried a simulation with abnormally high coupling resistance (138 times our "normal" value). The characteristic length scale is no longer much larger than the simulation cell spacing (here, 100 μm), so individual cells now express themselves. We find the conduction velocity is very much slowed (1.1 cm/s), as expected, and the overall size of the spiral wave is much smaller. The spiral wave core as viewed in terms of the depressed calcium concentration now consists of only about eight simulation cells. Meandering of the spiral wave is again present, this time apparently caused by cell discreteness. As the calcium-depressed core moves away from individual cells, those cells are then hit by sodium-influx wavefronts, causing abnormally large induced calcium releases and correspondingly large, transitory increases in the local intracellular calcium concentration. The effects of these observed phenomena on the dynamics of the wave have yet to be ascertained.

Our preliminary two-dimensional LRd simulations have thus exhibited many of the features we will be interested in investigating in the future, including spiral wave stability and meandering, large variations in spiral wave parameters, such as phase velocity, duration of the period between action potentials, and rotation period, and many effects due specifically to the LRd ion channel dynamics, such as those relating to the excitablity, membrane potential, and dynamics of the spiral core or center of rotation.

6. SUMMARY

Computer simulations of problems arising outside the physics mainstream often require computational techniques equal in complexity to those involved in more traditional areas of

physics and applied physics. The study of cardiac bioelectricity is one such area. While the problems in this area involve an understanding of fields such as physiology and cardiology, a surprising number of fields familiar to computational physicists turn out to be quite useful. These include an understanding of numerical methods, dynamical systems, ordinary and partial differential equation theory, theory of electromagnetic fields and electrodynamics, statistical mechanics and probability theory, and fluid dynamics. In this brief exposition, we have demonstrated how knowledge of the diffusion equation combined with nonlinear dynamics leads to a basic understanding of how action potentials propagate, how they annihilate one another, and how they form complex patterns such as spiral waves. Numerically, we have seen how a familiarity with the notions of timestepping, finite differencing, linear interpolation, method accuracy, and stability leads to an algorithm which efficiently handles the disparate timescales existing at different times and different places in the simulation. We have seen how basic computer structures such as binary trees and rectangular grids may be combined to provide an effective implementation of the chosen numerical algorithm. Such a relationship in turn demonstrates how a computational physicist can be useful in other fields, and conversely, how these fields can be fertile ground for problems of interest to the computational physicist.

ACKNOWLEDGMENTS

I am grateful for the guidance I have received in this new field from R. F. Gilmour, Jr., and Y. Rudy. Also, thanks to G. Oster and A. Winfree for getting me started in this field. D. Allexandre was instrumental in developing background material for this article. I also acknowledge helpful conversations with R. Lamb.

REFERENCES

1. M. A. Allessie, F. I. M. Bonke, and F. J. G. Schopman, Circus movement in rabbit atrial muscle as a mechanism of tachycardia. III. The “leading circle” concept: A new model of circus movement in cardiac tissue without the involvement of an anatomical obstacle, *Circ. Res.* **41**, 9 (1977).
2. D. Barkley, M. Kness, and L. S. Tuckerman, Spiral wave dynamics in a simple model of excitable media: The transition from simple to compound rotation, *Phys. Rev. A* **42**, 2489 (1990).
3. O. Berenfeld and A. M. Pertsov, Dynamics of intramural scroll waves in three-dimensional continuous myocardium with rotational anisotropy, *J. Theoret. Biol.* **1999**, 383 (1999).
4. *Chaos* **8**, 1 (1998).
5. S. M. Dillon, M. A. Allessie, P. C. Ursell, and A. L. Wit, Influences of anisotropic tissue structure on reentrant circuits in the epicardial border zone of subacute canine infarcts, *Circ. Res.* **63**, 182 (1988).
6. I. R. Efimov, V. I. Krinsky, and J. Jalife, Dynamics of rotating vorticies in the Beeler–Reuter model of cardiac tissue, *Chaos Solitons Fractals* **5**, 513 (1995).
7. N. El-Sherif, Reentrant mechanisms in ventricular arrhythmias, in *Cardiac Electrophysiology: From Cell to Bedside*, edited by D. P. Zipes and J. Jalife (Saunders, Philadelphia, 1995), 2nd ed., p. 567.
8. F. Fenton and A. Karma, Vortex dynamics in three-dimensional continuous myocardium with fiber rotation: Filament instability and fibrillation, *Chaos* **8**, 20 (1998).
9. R. A. FitzHugh, Impulses and physiological states in theoretical models of nerve membrane, *Biophys. J.* **1**, 445 (1961).
10. C. W. Gear, *Numerical Initial Value Problems in Ordinary Differential Equations* (Prentice Hall, New York, 1971), p. 155.
11. A. C. Guyton and J. E. Hall, *Textbook of Medical Physiology* (Saunders, Philadelphia, 1995).
12. D. M. Harrild and C. S. Henriquez, A finite volume model of cardiac propagation, *Ann. Biomed. Eng.* **25**, 315 (1997).

13. J. P. Keener and J. J. Tyson, The dynamics of scroll waves in excitable media, *SIAM Rev.* **34**, (1992).
14. J. P. Keener and A. V. Panfilov, Three dimensional propagation in the heart: The effects of geometry and fiber orientation on propagation in myocardium, in *Cardiac Electrophysiology: From Cell to Bedside*, edited by D. P. Zipes and J. Jalife (Saunders, Philadelphia, 1995), 2nd ed., p. 335.
15. L. J. Leon and F. A. Roberge, Structural complexity effects on transverse propagation in a two-dimensional model of myocardium, *IEEE Trans. Biomed. Eng.* **38**, 997 (1991).
16. C.-H. Luo and Y. Rudy, A dynamic model of the cardiac ventricular action potential. I. Simulations of ionic currents and concentration changes, *Circ. Res.* **74**, 1071 (1994).
17. C.-H. Luo and Y. Rudy, A dynamic model of the cardiac ventricular action potential. II. Afterdepolarizations, triggered activity, and potentiation, *Circ. Res.* **74**, 1097 (1994).
18. J. Nagumo, S. Arimoto, and S. Yoshizawa, An active pulse transmission line simulating nerve axon, *Proc. IRE* **50**, 2061 (1962).
19. N. F. Otani and R. Hwa, Topological considerations in the generation of scroll waves in excitable and cyclical media, *Physica D* **77**, 434 (1994).
20. A. E. Pollard, N. Hooke, and C. S. Henriquez, Cardiac propagation simulation, *Crit. Rev. Biomed. Eng.* **20**, 171 (1992).
21. Z. Qu, J. N. Weiss, and A. Garfinkel, Cardiac electrical restitution properties and stability of reentrant spiral waves: A simulation study, *Am. J. Physiol.* **276** (*Heart. Circ. Physiol.* **45**), H269 (1999).
22. W. Quan, S. J. Evans, and H. M. Hastings, Efficient integration of a realistic two-dimensional cardiac tissue model by domain decomposition, *IEEE Trans. Biomed. Eng.* **45**, 372 (1998).
23. J. M. Rogers and A. D. McCulloch, A collocation-Galerkin finite element model of cardiac action potential propagation, *IEEE Trans. Biomed. Eng.* **41**, 743 (1994).
24. B. J. Roth, Frequency locking of meandering spiral waves in cardiac tissue, *Phys. Rev. E* **57**, R3735 (1998).
25. S. Rush and H. Larsen, A practical algorithm for solving dynamic membrane equations, *IEEE Trans. Biomed. Eng.* **25**, 389 (1978).
26. H. I. Saleheen and K. T. Ng, A new three-dimensional finite-difference bidomain formulation for inhomogeneous anisotropic cardiac tissues, *IEEE Trans. Biomed. Eng.* **45**, 15 (1998).
27. R. M. Shaw and Y. Rudy, Ionic mechanisms of propagation in cardiac tissue: Roles of the sodium and L-type calcium currents during reduced excitability and decreased gap junction coupling, *Circ. Res.* **81**, 727 (1997).
28. E. J. Vigmond and L. J. Leon. Computationally efficient model for simulating electrical activity in cardiac tissue with fiber rotation, *Ann. Biomed. Eng.* **27**, 160 (1999).
29. A. T. Winfree, Theory of spirals, in *Cardiac Electrophysiology: From Cell to Bedside*, edited by D. P. Zipes and J. Jalife (Saunders, Philadelphia, 1995), 2nd ed., p. 379.
30. A. T. Winfree, Sudden cardiac death: A problem in topology, *Sci. Am.* **144** (1983).
31. J. Zeng, K. R. Laurita, D. S. Rosenbaum, and Y. Rudy, Two components of the delayed rectifier K^+ current in ventricular myocytes of the guinea pig type, theoretical formulation and their role in repolarization, *Circ. Res.* **77**, 140 (1995).
32. D. P. Zipes and J. Jalife, *Cardiac Electrophysiology: From Cell to Beside* (Saunders, Philadelphia, 1995), 2nd ed.